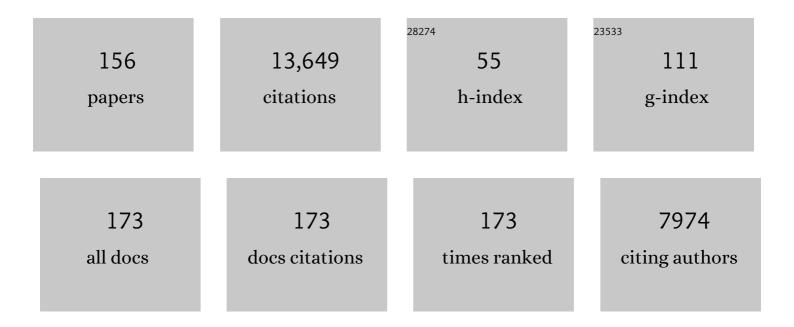
## Richard A Ketcham

List of Publications by Year in descending order

Source: https://exaly.com/author-pdf/3711341/publications.pdf Version: 2024-02-01



#	Article	IF	CITATIONS
1	Predictive digital rock physics without segmentation. Computers and Geosciences, 2022, 159, 105008.	4.2	2
2	Orogenic gold ores in three-dimensions: A case study of distinct mineralization styles at the world-class Cuiabá deposit, Brazil, using high-resolution X-ray computed tomography on gold particles. Ore Geology Reviews, 2022, 140, 104584.	2.7	5
3	Short communication: Modeling competing effects of cooling rate, grain size, and radiation damage in low-temperature thermochronometers. Geochronology, 2022, 4, 143-152.	2.5	11
4	From Left Slip to Transpression: Cenozoic Tectonic Evolution of the North Altyn Fault, NW Margin of the Tibetan Plateau. Tectonics, 2022, 41, .	2.8	10
5	Role of Defects and Radiation Damage on He Diffusion in Magnetite: Implication for (U-Th)/He Thermochronology. Minerals (Basel, Switzerland), 2022, 12, 590.	2.0	6
6	3D porosity structure of the earliest solar system material. Scientific Reports, 2022, 12, 8369.	3.3	2
7	Seamless low-temperature thermochronological modeling in Andino 3D, towards integrated structural and thermal simulations. Journal of South American Earth Sciences, 2021, 105, 102851.	1.4	5
8	Thermo-kinematic modeling of detachment-dominated extension, northeastern Death Valley area, USA: Implications for mid-crustal thermal-rheological evolution. Tectonophysics, 2021, 808, 228755.	2.2	7
9	Confined fission-track revelation in apatite: how it works and why it matters. Geochronology, 2021, 3, 433-464.	2.5	4
10	Comment on the reply to the Comment on "Thermal history modelling: HeFTy vs. QTQt―by Vermeesch and Tian, Earth-Science Reviews (2014), 139, 279–290. Earth-Science Reviews, 2020, 203, 102878.	9.1	12
11	A multi-method, multi-scale theoretical study of He and Ne diffusion in zircon. Geochimica Et Cosmochimica Acta, 2020, 268, 348-367.	3.9	22
12	The along-track etching structure of fission tracks in apatite: Observations and implications. Chemical Geology, 2020, 553, 119809.	3.3	9
13	The Complexity of Nonlinear Flow and nonâ€Fickian Transport in Fractures Driven by Threeâ€Dimensional Recirculation Zones. Journal of Geophysical Research: Solid Earth, 2020, 125, e2020JB020028.	3.4	30
14	Unraveling the exhumation history of high-pressure ophiolites using magnetite (U-Th-Sm)/He thermochronometry. Earth and Planetary Science Letters, 2020, 543, 116359.	4.4	15
15	Simulating effects of heterogeneous 4He concentration profiles and radiation damage annealing on whole-grain zircon diffusivity analyses. Geochimica Et Cosmochimica Acta, 2020, 284, 239-253.	3.9	4
16	ls Lowâ€Temperature Fissionâ€Track Annealing in Apatite a Thermally Controlled Process?. Geochemistry, Geophysics, Geosystems, 2020, 21, e2019GC008877.	2.5	14
17	Andean Mountain Building and Foreland Basin Evolution During Thin―and Thickâ€Skinned Neogene Deformation (32–33°S). Tectonics, 2020, 39, e2019TC005838.	2.8	21
18	Analyst and etching protocol effects on the reproducibility of apatite confined fission-track length measurement, and ambient-temperature annealing at decadal timescales. American Mineralogist, 2019, 104, 1421-1435.	1.9	12

#	Article	IF	CITATIONS
19	4D Imaging of Mineral Dissolution in Porous Carbonado Diamond: Implications for Acid Digestion and XCT Measurement of Porosity and Material Properties. Frontiers in Earth Science, 2019, 7, .	1.8	4
20	Reply to: Charlier etÂal. 2018. Mudslide and/or animal attack are more plausible causes and circumstances of death for AL 288 (â€~Lucy'): a forensic anthropology analysis. <i>Medico-Legal Journal</i> 86(3) 139–142, 2018. Medico-Legal Journal, 2019, 87, 121-126.	0.5	1
21	Accurate Measurement of Small Features in Xâ€Ray CT Data Volumes, Demonstrated Using Gold Grains. Journal of Geophysical Research: Solid Earth, 2019, 124, 3508-3529.	3.4	19
22	Water flow, oil biodegradation, and hydrodynamic traps in the Llanos Basin, Colombia. AAPG Bulletin, 2019, 103, 1225-1264.	1.5	4
23	Mass-transfer based modeling to investigate iodine staining effects for enhanced contrast X-ray computed tomography. Palaeoworld, 2019, 28, 562-571.	1.1	2
24	Fission-Track Annealing: From Geologic Observations to Thermal History Modeling. Springer Textbooks in Earth Sciences, Geography and Environment, 2019, , 49-75.	0.3	37
25	Resolution-invariant measurements of small objects in polychromatic CT data. , 2019, , .		1
26	Numerically estimating rock frame properties of a mixed calcite and dolomite hand sample using computed tomography (CT). , 2019, , .		1
27	Resolving the effects of 2-D versus 3-D grain measurements on apatite (U–Th) â^ He age data and reproducibility. Geochronology, 2019, 1, 17-41.	2.5	40
28	Comment on "Thermal history modelling: HeFTy vs. QTQt―by Vermeesch and Tian, Earth-Science Reviews (2014), 139, 279–290. Earth-Science Reviews, 2018, 176, 387-394.	9.1	26
29	Deciphering exhumation and burial history with multiâ€sample downâ€well thermochronometric inverse modelling. Basin Research, 2018, 30, 48-64.	2.7	26
30	Evidence for accretion of fine-grained rims in a turbulent nebula for CM Murchison. Earth and Planetary Science Letters, 2018, 481, 201-211.	4.4	31
31	Reproducibility of Thermal History Reconstruction From Apatite Fissionâ€Track and (Uâ€Th)/He Data. Geochemistry, Geophysics, Geosystems, 2018, 19, 2411-2436.	2.5	31
32	Latitudinal and Longitudinal Patterns of Exhumation in the Andes of Northâ€Central Chile. Tectonics, 2018, 37, 2863-2886.	2.8	23
33	X-ray computed tomography of planetary materials: A primer and review of recent studies. Chemie Der Erde, 2017, 77, 547-572.	2.0	89
34	Does trabecular bone structure within the metacarpal heads of primates vary with hand posture?. Comptes Rendus - Palevol, 2017, 16, 533-544.	0.2	21
35	X-ray computed tomography datasets for forensic analysis of vertebrate fossils. Scientific Data, 2016, 3, 160040.	5.3	7
36	Response to comment on "A reporting protocol for thermochronologic modeling illustrated with data from the Grand Canyon― Earth and Planetary Science Letters, 2016, 441, 213.	4.4	9

#	Article	IF	CITATIONS
37	Andean topographic growth and basement uplift in southern Colombia: Implications for the evolution of the Magdalena, Orinoco, and Amazon river systems. , 2016, 12, 1235-1256.		67
38	Perimortem fractures in Lucy suggest mortality from fall out of tall tree. Nature, 2016, 537, 503-507.	27.8	67
39	Comparison and Evaluation of the Effectiveness of Two Approaches of Diffusible Iodineâ€Based Contrastâ€Enhanced Computed Tomography (diceCT) for Avian Cephalic Material. Journal of Experimental Zoology Part B: Molecular and Developmental Evolution, 2016, 326, 352-362.	1.3	20
40	Movement vectors and deformation mechanisms in kinematic restorations: A case study from the Colombian Eastern Cordillera. Interpretation, 2016, 4, T31-T48.	1.1	18
41	Limb Bone Structural Proportions and Locomotor Behavior in A.L. 288-1 ("Lucy"). PLoS ONE, 2016, 11, e0166095.	2.5	78
42	Modification of the <scp>L</scp> ocal <scp>C</scp> ubic <scp>L</scp> aw of fracture flow for weak inertia, tortuosity, and roughness. Water Resources Research, 2015, 51, 2064-2080.	4.2	149
43	An investigation of the efficacy and mechanism of contrast-enhanced X-ray Computed Tomography utilizing iodine for large specimens through experimental and simulation approaches. BMC Physiology, 2015, 15, 5.	3.6	31
44	Wettability measurement under high <scp>P</scp> â€ <scp>T</scp> conditions using <scp>X</scp> â€ray imaging with application to the brineâ€supercritical <scp>C</scp> O <sub>2</sub> system. Geochemistry, Geophysics, Geosystems, 2015, 16, 2858-2864.	2.5	21
45	High-resolution 3D analyses of the shape and internal constituents of small volcanic ash particles: The contribution of SEM micro-computed tomography (SEM micro-CT). Journal of Volcanology and Geothermal Research, 2015, 293, 1-12.	2.1	31
46	3-D X-ray tomography of diamondiferous mantle eclogite xenoliths, Siberia: A review. Journal of Asian Earth Sciences, 2015, 101, 39-67.	2.3	15
47	Technical Note: Calculation of stoichiometry from EMP data for apatite and other phases with mixing on monovalent anion sites. American Mineralogist, 2015, 100, 1620-1623.	1.9	83
48	Inter-laboratory comparison of fission track confined length and etch figure measurements in apatite. American Mineralogist, 2015, 100, 1452-1468.	1.9	38
49	Coupling sequential restoration of balanced cross sections and low-temperature thermochronometry: The case study of the Western Carpathians. Lithosphere, 2015, 7, 367-378.	1.4	23
50	Kinematic restoration of contractional basement structures using thermokinematic models: A key tool for petroleum system modeling. AAPG Bulletin, 2015, 99, 1575-1598.	1.5	37
51	FetKin: Coupling kinematic restorations and temperature to predict thrusting, exhumation histories, and thermochronometric ages. AAPG Bulletin, 2015, 99, 1557-1573.	1.5	21
52	A reporting protocol for thermochronologic modeling illustrated with data from the Grand Canyon. Earth and Planetary Science Letters, 2015, 432, 425-435.	4.4	99
53	Impact-induced brittle deformation, porosity loss, and aqueous alteration in the Murchison CM chondrite. Geochimica Et Cosmochimica Acta, 2015, 171, 256-282.	3.9	48
54	Application of high resolution X-ray computed tomography to mineral deposit origin, evaluation, and processing. Ore Geology Reviews, 2015, 65, 821-839.	2.7	95

#	Article	IF	CITATIONS
55	Formation of passive-roof duplexes in the Colombian Subandes and Perú. Lithosphere, 2014, 6, 456-472.	1.4	31
56	Mineralogy and petrography of C asteroid regolith: The Sutter's Mill <scp>CM</scp> meteorite. Meteoritics and Planetary Science, 2014, 49, 1997-2016.	1.6	57
57	Characterizing, measuring, and utilizing the resolution of CT imagery for improved quantification of fine-scale features. Nuclear Instruments & Methods in Physics Research B, 2014, 324, 80-87.	1.4	17
58	The secondary origin of diamonds: multi-modal radiation tomography of diamondiferous mantle eclogites. International Geology Review, 2014, 56, 1172-1180.	2.1	11
59	Beam hardening correction for X-ray computed tomography of heterogeneous natural materials. Computers and Geosciences, 2014, 67, 49-61.	4.2	61
60	Surface tension of hydrous silicate melts: Constraints on the impact of melt composition. Journal of Volcanology and Geothermal Research, 2013, 267, 68-74.	2.1	32
61	Crystallization kinetics during regional metamorphism of porphyroblastic rocks. Journal of Metamorphic Geology, 2013, 31, 963-979.	3.4	24
62	Chemical influence on α-recoil damage annealing in apatite: Implications for (U–Th)/He dating. Chemical Geology, 2013, 351, 257-267.	3.3	90
63	Magnitudes of departures from equilibrium during regional metamorphism of porphyroblastic rocks. Journal of Metamorphic Geology, 2013, 31, 981-1002.	3.4	27
64	Helium diffusion in natural zircon: Radiation damage, anisotropy, and the interpretation of zircon (U-Th)/He thermochronology. Numerische Mathematik, 2013, 313, 145-198.	1.4	516
65	Geometric analysis of radiation damage connectivity in zircon, and its implications for helium diffusion. American Mineralogist, 2013, 98, 350-360.	1.9	69
66	On the lag time between internal strain and basement involved thrust induced exhumation: The case of the Colombian Eastern Cordillera. Journal of Structural Geology, 2013, 52, 96-118.	2.3	21
67	Computational Fluid Dynamics Simulation of Structured Packing. Industrial & Engineering Chemistry Research, 2013, 52, 2032-2045.	3.7	43
68	New textural evidence on the origin of carbonado diamond: An example of 3-D petrography using X-ray computed tomography. , 2013, 9, 1336-1347.		13
69	Poreâ€scale trapping of supercritical CO <sub>2</sub> and the role of grain wettability and shape. Geophysical Research Letters, 2013, 40, 3878-3882.	4.0	132
70	Investigation of the swelling behavior of Dome Matrix drug delivery modules by high-resolution X-ray computed tomography. Journal of Drug Delivery Science and Technology, 2013, 23, 165-170.	3.0	9
71	Analysis of Three-dimensional Geometrical Pore Parameters From Rock Weathering. Soil Science, 2012, 177, 506-516.	0.9	4
72	Kinematic evolution of Andean foldâ€ŧhrust structures along the boundary between the Eastern Cordillera and Middle Magdalena Valley basin, Colombia. Tectonics, 2012, 31, .	2.8	30

#	Article	IF	CITATIONS
73	Numerical simulation of diffusion ontrolled nucleation and growth of porphyroblasts. Journal of Metamorphic Geology, 2012, 30, 489-512.	3.4	25
74	Accounting for long alpha-particle stopping distances in (U–Th–Sm)/He geochronology: 3D modeling of diffusion, zoning, implantation, and abrasion. Geochimica Et Cosmochimica Acta, 2012, 96, 44-56.	3.9	96
75	Visualization of anomalous penetrant transport in glassy poly(methyl methacrylate) utilizing high-resolution X-ray computed tomography. Polymer, 2012, 53, 776-781.	3.8	4
76	Basin Thermal History Analysis Using (U-Th)/He Thermochronometry. , 2012, , 105-123.		1
77	U and Th zonation in apatite observed by laser ablation ICPMS, and implications for the (U–Th)/He system. Geochimica Et Cosmochimica Acta, 2011, 75, 4515-4530.	3.9	111
78	Accounting for long alpha-particle stopping distances in (U–Th–Sm)/He geochronology: Refinement of the baseline case. Geochimica Et Cosmochimica Acta, 2011, 75, 7779-7791.	3.9	247
79	Solid modeling of fossil small mammal teeth. Computers and Geosciences, 2011, 37, 1364-1371.	4.2	8
80	Bubble nucleation in rhyolite and dacite melts: temperature dependence of surface tension. Contributions To Mineralogy and Petrology, 2011, 162, 929-943.	3.1	65
81	Trabecular bone structure in the mandibular condyles of gouging and nongouging platyrrhine primates. American Journal of Physical Anthropology, 2010, 141, 583-593.	2.1	23
82	Comparative forefoot trabecular bone architecture in extant hominids. Journal of Human Evolution, 2010, 59, 202-213.	2.6	59
83	Three-dimensional measurement of fractures in heterogeneous materials using high-resolution X-ray computed tomography. , 2010, 6, 499-514.		106
84	Migration of Cenozoic deformation in the Eastern Cordillera of Colombia interpreted from fission track results and structural relationships: Implications for petroleum systems. AAPG Bulletin, 2010, 94, 1543-1580.	1.5	101
85	An X-ray computed tomography study of inclusion trail orientations in multiple porphyroblasts from a single sample. Tectonophysics, 2010, 480, 305-320.	2.2	25
86	Mineralogy and petrography of the Almahata Sitta ureilite. Meteoritics and Planetary Science, 2010, 45, 1618-1637.	1.6	74
87	Metasomatic origin of diamonds in the world's largest diamondiferous eclogite. Lithos, 2009, 112, 1014-1024.	1.4	45
88	Patterns in ontogeny of human trabecular bone from SunWatch Village in the Prehistoric Ohio Valley: General features of microarchitectural change. American Journal of Physical Anthropology, 2009, 138, 318-332.	2.1	81
89	Flow Field Visualization in Structured Packing Using Real Time X-ray Radiography. Industrial & Engineering Chemistry Research, 2009, 48, 3606-3618.	3.7	7
90	Reproducibility of apatite fission-track length data and thermal history reconstruction. Earth and Planetary Science Letters, 2009, 284, 504-515.	4.4	134

#	Article	IF	CITATIONS
91	Annealing behavior of alpha recoil tracks in phlogopite. Chemical Geology, 2009, 266, 343-349.	3.3	7
92	Apatite (U–Th)/He thermochronometry using a radiation damage accumulation and annealing model. Geochimica Et Cosmochimica Acta, 2009, 73, 2347-2365.	3.9	732
93	Effects of inertia and directionality on flow and transport in a rough asymmetric fracture. Journal of Geophysical Research, 2009, 114, .	3.3	74
94	High resolution X-ray computed tomography studies of Grasberg porphyry Cu-Au ores, Papua, Indonesia. Mineralium Deposita, 2008, 43, 519-532.	4.1	31
95	Formation of garnet polycrystals during metamorphic crystallization. Journal of Metamorphic Geology, 2008, 26, 365-383.	3.4	28
96	The formation and chronology of the PAT 91501 impact-melt L chondrite with vesicle–metal–sulfide assemblages. Geochimica Et Cosmochimica Acta, 2008, 72, 2417-2428.	3.9	38
97	The unroofing history of Naxos and Paros: Constraints and questions from thermochronology and thermal modeling. IOP Conference Series: Earth and Environmental Science, 2008, 2, 012019.	0.3	0
98	Using Highâ€Resolution Computed Tomography Analysis To Characterize Soilâ€5urface Seals. Soil Science Society of America Journal, 2008, 72, 1478-1485.	2.2	26
99	Improved measurement of fission-track annealing in apatite using c-axis projection. American Mineralogist, 2007, 92, 789-798.	1.9	234
100	Novel Application of X-ray Computed Tomography:  Determination of Gas/Liquid Contact Area and Liquid Holdup in Structured Packing. Industrial & Engineering Chemistry Research, 2007, 46, 5734-5753.	3.7	48
101	Improved modeling of fission-track annealing in apatite. American Mineralogist, 2007, 92, 799-810.	1.9	719
102	Navier‣tokes flow and transport simulations using real fractures shows heavy tailing due to eddies. Geophysical Research Letters, 2007, 34, .	4.0	120
103	Nonhuman anthropoid primate femoral neck trabecular architecture and its relationship to locomotor mode. Anatomical Record, 2007, 290, 422-436.	1.4	87
104	Origin and mechanical significance of honeycomb garnet in high-pressure metasedimentary rocks from the Tauern Window, Eastern Alps. Journal of Metamorphic Geology, 2007, 25, 565-583.	3.4	29
105	Methodology for Evaluating Candidate Geometric Reference Scaffolds. Journal of Testing and Evaluation, 2007, 35, 100598.	0.7	Ο
106	Late Mesozoic and Cenozoic thermotectonic evolution along a transect from the north China craton through the Qinling orogen into the Yangtze craton, central China. Tectonics, 2006, 25, n/a-n/a.	2.8	101
107	Constraining the long-term evolution of the slip rate for a major extensional fault system in the central Aegean, Greece, using thermochronology. Earth and Planetary Science Letters, 2006, 241, 293-306.	4.4	123
108	Formation of vesicles in asteroidal basaltic meteorites. Earth and Planetary Science Letters, 2006, 246, 102-108.	4.4	41

#	Article	IF	CITATIONS
109	Three-dimensional reconstruction of enamel thickness and volume in humans and hominoids. European Journal of Oral Sciences, 2006, 114, 360-364.	1.5	22
110	Preliminary observations on the calcaneal trabecular microarchitecture of extant large-bodied hominoids. American Journal of Physical Anthropology, 2006, 129, 410-417.	2.1	74
111	New algorithms for ring artifact removal. , 2006, 6318, 216.		38
112	Utility of high resolution xâ€ray computed tomography (HRXCT) for paleobotanical studies: an example using London Clay fruits and seeds. American Journal of Botany, 2006, 93, 1848-1851.	1.7	32
113	Hoax or History: A Bison Skull with Embedded Calf Creek Projectile Point. Plains Anthropologist, 2005, 50, 221-226.	0.3	3
114	The role of crystallographic angle in characterizing and modeling apatite fission-track length data. Radiation Measurements, 2005, 39, 595-601.	1.4	27
115	Definitive fossil evidence for the extant avian radiation in the Cretaceous. Nature, 2005, 433, 305-308.	27.8	305
116	Three-dimensional grain fabric measurements using high-resolution X-ray computed tomography. Journal of Structural Geology, 2005, 27, 1217-1228.	2.3	201
117	Angular orientation of trabecular bone in the femoral head and its relationship to hip joint loads in leaping primates. Journal of Morphology, 2005, 265, 249-263.	1.2	76
118	Organization of the Olfactory and Respiratory Skeleton in the Nose of the Gray Short-Tailed Opossum Monodelphis domestica. Journal of Mammalian Evolution, 2005, 12, 303-336.	1.8	95
119	3. Apatite Fission-Track Analysis. , 2005, , 49-94.		46
120	11. Forward and Inverse Modeling of Low-Temperature Thermochronometry Data. , 2005, , 275-314.		90
121	Improved methods for quantitative analysis of three-dimensional porphyroblastic textures. , 2005, 1, 42.		31
122	Getting the inside story: using computed X-ray tomography to study inclusion trails in garnet porphyroblasts. American Mineralogist, 2005, 90, ea1-ea17.	1.9	15
123	Computational methods for quantitative analysis of three-dimensional features in geological specimens. , 2005, 1, 32.		279
124	Apatite Fission-Track Analysis. Reviews in Mineralogy and Geochemistry, 2005, 58, 49-94.	4.8	505
125	Forward and Inverse Modeling of Low-Temperature Thermochronometry Data. Reviews in Mineralogy and Geochemistry, 2005, 58, 275-314.	4.8	949
126	Computational Tools for Low-Temperature Thermochronometer Interpretation. Reviews in Mineralogy and Geochemistry, 2005, 58, 589-622.	4.8	139

#	Article	IF	CITATIONS
127	Nondestructive high-resolution visualization and measurement of anisotropic effective porosity in complex lithologies using high-resolution X-ray computed tomography. Journal of Hydrology, 2005, 302, 92-106.	5.4	102
128	Quantification and visualization of anisotropy in trabecular bone. Journal of Microscopy, 2004, 213, 158-171.	1.8	150
129	The avian nature of the brain and inner ear of Archaeopteryx. Nature, 2004, 430, 666-669.	27.8	188
130	Structure and function of the horn shark (Heterodontus francisci) cranium through ontogeny: Development of a hard prey specialist. Journal of Morphology, 2004, 260, 1-12.	1.2	79
131	A uniquely specialized ear in a very early tetrapod. Nature, 2003, 425, 65-69.	27.8	95
132	From CT scans of embedded Ivanovia to models using rapid prototyping. Palaeontology, 2003, 46, 839-843.	2.2	6
133	Observations on the relationship between crystallographic orientation and biasing in apatite fission-track measurements. American Mineralogist, 2003, 88, 817-829.	1.9	45
134	Applications of high-resolution X-ray computed tomography in petrology, meteoritics and palaeontology. Geological Society Special Publication, 2003, 215, 7-22.	1.3	47
135	IN SITU DISTRIBUTION OF GOLD IN ORES USING HIGH-RESOLUTION X-RAY COMPUTED TOMOGRAPHY. Economic Geology, 2003, 98, 1697-1701.	3.8	24
136	High-resolution X-ray computed tomography of impactites. Journal of Geophysical Research, 2002, 107, 19-1.	3.3	20
137	The three-dimensional structure of trabecular bone in the femoral head of strepsirrhine primates. Journal of Human Evolution, 2002, 43, 1-26.	2.6	132
138	Femoral head trabecular bone structure in two omomyid primates. Journal of Human Evolution, 2002, 43, 241-263.	2.6	91
139	Calsoyasuchus valliceps, a new crocodyliform from the Early Jurassic Kayenta Formation of Arizona. Journal of Vertebrate Paleontology, 2002, 22, 593-611.	1.0	105
140	The Archaeoraptor forgery. Nature, 2001, 410, 539-540.	27.8	72
141	Acquisition, optimization and interpretation of X-ray computed tomographic imagery: applications to the geosciences. Computers and Geosciences, 2001, 27, 381-400.	4.2	1,172
142	High-Resolution X-ray Computed Tomography as a Tool for Visualization and Quantitative Analysis of Igneous Textures in Three Dimensions. Visual Geosciences, 2000, 4, 1-14.	0.5	13
143	Nondestructive evaluation of cavitation in an Al–Mg material deformed under creep conditions. Journal of Materials Research, 2000, 15, 76-84.	2.6	7
144	Variability of apatite fission-track annealing kinetics; II, Crystallographic orientation effects. American Mineralogist, 1999, 84, 1224-1234.	1.9	355

#	Article	IF	CITATIONS
145	Variability of apatite fission-track annealing kinetics; I, Experimental results. American Mineralogist, 1999, 84, 1213-1223.	1.9	492
146	Variability of apatite fission-track annealing kinetics; III, Extrapolation to geological time scales. American Mineralogist, 1999, 84, 1235-1255.	1.9	656
147	Three-dimensional quantitative textural analysis of metamorphic rocks using high-resolution computed X-ray tomography: Part I. Methods and techniques. Journal of Metamorphic Geology, 1997, 15, 29-44.	3.4	175
148	Thermal models of core-complex evolution in Arizona and New Guinea: Implications for ancient cooling paths and present-day heat flow. Tectonics, 1996, 15, 933-951.	2.8	61
149	An improved method for determination of heat production with gamma-ray scintillation spectrometry. Chemical Geology, 1996, 130, 175-194.	3.3	24
150	Distribution of heat-producing elements in the upper and middle crust of southern and west central Arizona: Evidence from the core complexes. Journal of Geophysical Research, 1996, 101, 13611-13632.	3.3	70
151	Controls on the nucleation and growth of porphyroblasts: Kinetics from natural textures and numerical models. Geological Journal, 1995, 30, 207-225.	1.3	102
152	Effects of temperature-dependent material properties and radioactive heat production on simple basin subsidence models. Earth and Planetary Science Letters, 1995, 130, 31-44.	4.4	8
153	Thermal structure of active thrust belts. Journal of Metamorphic Geology, 1988, 6, 559-570.	3.4	37
154	Extracting Particle Orientations from Three-dimensional Datasets using BLOB3D. , 0, , 407-413.		3
155	Accurate Three-dimensional Measurements of Features in Geological Materials from X-ray Computed Tomography Data. , 0, , 143-148.		14
156	Intracontinental subduction beneath the Pamir Mountains: Constraints from thermokinematic modeling of shortening in the Tajik fold-and-thrust belt. Bulletin of the Geological Society of America, 0, , .	3.3	18